Tin Oxide Nanowires, Nanoribbons, and Nanotubes

Z. R. Dai,[†] J. L. Gole,[‡] J. D. Stout,[‡] and Z. L. Wang*[,†]

School of Materials Science and Engineering, Georgia Institute of Technology, Atlanta, Georgia 30332-0245 and School of Physics, Georgia Institute of Technology, Atlanta, Georgia 30332-0430

Received: August 18, 2001; In Final Form: October 26, 2001

Nanowires, sandwiched nanoribbons, and nanotubes of SnO_2 are synthesized using elevated temperature synthesis techniques, and their structures are characterized in detail by scanning electron microscopy (SEM) and transmission electron microscopy (TEM). In addition to the normal rutile structured SnO_2, it has been possible to form an orthorhombic superlattice-like structure in the present study. The orthorhombic structure can form in a thin nanowire, coexist with the normal rutile structured SnO_2 in a sandwiched nanoribbon, or occur in the form of nanotubes. This result is distinct from that for bulk SnO_2 where pressures in excess of 150 kbar are required to form the orthorhombic form. The orientation relationship between the orthorhombic SnO_2 and the rutile structured SnO_2 is determined to be $[001]_o \parallel [10\bar{2}]_t$ and $(100)_o \parallel (010)_t$ for the nanowires and sandwiched nanoribbons, and $[001]_o \parallel [3\bar{1}7]_t$ and $(110)_o \parallel (451)_t$ for the nanotubes. Although the growth direction of the rutile structured SnO_2 nanowires is along $[101]_t$, two growth directions are found to occur in the nanostructures having the orthorhombic SnO_2 structure. They are $[010]_o$ for nanowires and $[\bar{1}10]_o$ for the sandwiched nanoribbons and nanotubes. The results in this study and the observation of orthorhombic SnO_2 may result from the formation of the products in an oxygen deficient environment.

1. Introduction

Searching for interconnects is a challenge to future nanoelectronics. With the reduction in feature size of devices, it is essential to find one-dimensional nanomaterials that can integrate these devices and interconnects. Semiconductor nanowires[1,2] and the recently discovered semiconducting oxide nanobelts[3,4] are potential candidates for fabrication of nanoscale devices using the integrity of the individual nanowires and belts. However, there is considerable additional potential for the oxides as they represent the most diverse class of materials, with properties covering almost all aspects of material science and physics in areas including superconductivity, ferroelectricity, magnetism, and more. Oxides are fundamental to smart and functional materials due to two unique characteristics: variation in valence state and oxygen vacancies. The synthesis techniques and the products we discuss here reflect especially the latter property.

Semiconducting and amphoteric SnO_2 is a key functional material that has been used extensively for optoelectronic devices[5,6] and gas sensors which detect leakages of reducing gases such as H, S, CO, and others.[7−12] Recently, a series of binary semiconducting oxide nanobelts (or nanoribbons), such as ZnO, In_2O_3, Ga_2O_3, CdO, and PbO_2 and including SnO_2 have been successfully synthesized by simply evaporating the source compound.[3−4,13] The source material used for the synthesis of SnO_2 nanobelts is primarily SnO_2 but also SnO powders. Stoichiometric SnO_2 nanobelts with a high quality rutile crystalline structure and uniform geometry have been synthesized.

In this paper, we report the synthesis and structures of SnO_2 nanowires, nanoribbons, and nanotubes produced using primarily layered mixtures of Sn foil and SnO powder or simply SnO powder as the source material under more stringent vacuum conditions. A detailed microstructure study of the synthesized SnO_2 nanowires, nanoribbons, and nanotubes have been carried out, and their growth directions and morphology have been determined. Besides the rutile structure, an orthorhombic structured SnO_2 has also been observed in the nanostructures. This is in contrast to its observation only in the high-pressure phase for bulk tin oxide.

2. Experimental Methods

The technique of high temperature thermal oxide synthesis[14] has been adopted to synthesis procedures which, in concert with the control of entrainment flow rates, reactant mixtures, and annealing procedures, has allowed the synthesis of silicon/silica based nanotubes and nanoarrays.[16] With some modification these synthesis techniques allow the formation of tin oxide (SnO_2) nanowires, nanoribbons and nanotubes through the use of SnO/Sn and SnO based mixtures in a double concentric alumina tube configuration heated to 1050−1150 °C in a Lindberg Blue tube furnace configuration.

The inner tube of the furnace is vacuum sealed by two water cooled stainless steel end pieces, attached and tightly lock-press fit against custom viton O-rings.[15] At one end of the furnace, for the present tin-based synthesis, ultrahigh purity nitrogen gas enters through the upstream stainless steel end piece, passes through a matched set of zirconia insulators to the central region of the inner tube oven, and flows over an alumina crucible containing the source Sn/SnO or SnO mixtures, usually at a flow rate of 100 sccm.[15] The total pressure in the inner tube can be changed from 200 to 800 Torr (attached bubbler), controlled by a mechanical pump attached to the inner alumina tube through a downstreamwater cooled stainless steel end piece. This end piece is mechanically attached to a water cooled plate,[15] whose temperature is adjustable, located at the fringes of the

* To whom correspondence should be addressed. E-mail: zhong.wang@mse.gatech.edu.

[†] School of Materials Science and Engineering, Georgia Institute of Technology, Atlanta.

[‡] School of Physics, Georgia Institute of Technology.

10.1021/jp013214r CCC: $22.00
Published on Web 01/12/2002

TABLE 1: List of the Samples and Synthesis Conditions Used in the Present Study

sample	source material	*T* (°C)	pressure (Torr)	collecting place
#1 (10/12/00) Figure 1(a)	Sn foil + SnO layered N_2 flow gas	1125	400	tube wall
#2 (10/11/00) Figure 1(b)	Sn foil + SnO layered N_2 flow gas	1125	200	tube wall
#3 (10/11/00) Figure 1(c)	Sn foil + SnO layered N_2 flow gas	1125	200	cold plate 35−40 °C
#4 (4/20/00) Figure 2	Sn foil + SnO layered Ar flow gas	1050	200	tube wall
#5 (5/31/00) Figure 3, Figure 7 Figure 8	SnO powder $+N_2$ entrainment	1050	250−700	cold plate 25−40 °C
#6 (Likely 10/11) Figure 5, Figure 6	Sn foil + SnO layered N_2 flow gas	1125	200	cold plate 25−40 °C
#7 (6/21/00) Figure 1(a)	SnO powder N_2 entrainment	1100	255−500	tube wall

tube furnace hot zone. The entrance and exit regions of the alumina tube are insulated by a machined set of zirconia blocks.[15] A light to dark gray fluffy product is collected on the alumina tube wall near the point where the double concentric alumina tube configuration exits the Lindberg oven and where the temperature is in the range between 450 and 500 °C. Additional products are collected on the cold plate which is positioned ~6 in. into the tube furnace, fronting the upstream zirconia insulator. This cold plate is maintained at a temperature of 25−40 °C.

If the fluffy gray to gray-black, SnO_x, product is heated slowly to 1100 °C at P_{total} ~200 Torr under oxidative conditions (1% O_2 seeded argon) using a crucible directed concentric nozzle flow configuration, we observe its complete conversion to a white powder-like product which is more dense and consistent with bulk SnO_2. Further, if this same fluffy gray product is heated slowly under a reducing atmosphere (Ar/4% H_2 @ 1100 °C) it is converted completely to metallic tin. The conditions for the synthesis of all the product materials discussed in the following sections are presented in Table 1.

The as-synthesized products are characterized by scanning electron microscopy (SEM) (Hitachi S-800 FEG), transmission electron microscopy (TEM) (Hitachi HF-2000 FEG with energy-dispersive X-ray spectroscopy (EDS)) at 200 kV and a JEOL 4000EX high-resolution TEM (HRTEM) at 400 kV.

3. Results and Discussion

3.1 Morphology. The as-synthesized products were first inspected using SEM. Figure 1(a) depicts a typical distribution in morphology for the fluffy gray products collected on the wall of the alumina tube furnace following an SnO/Sn based synthesis. It is evident that the products are dominated by wire-like structures whose diameter varies over a broad range from several tens of nanometers to a micrometer. The typical length of the wires ranges from several tens to several hundred micrometers. The cross sectional shape of the wires can vary from virtually circular to the larger rectangle-like structure indicated by a white arrowhead in the enlarged SEM image (Figure 1(b)). The chemical composition of the wires is determined by EDS to be close to SnO_2. In addition to the wire-like structures, Figure 1(c) demonstrates that disklike structures

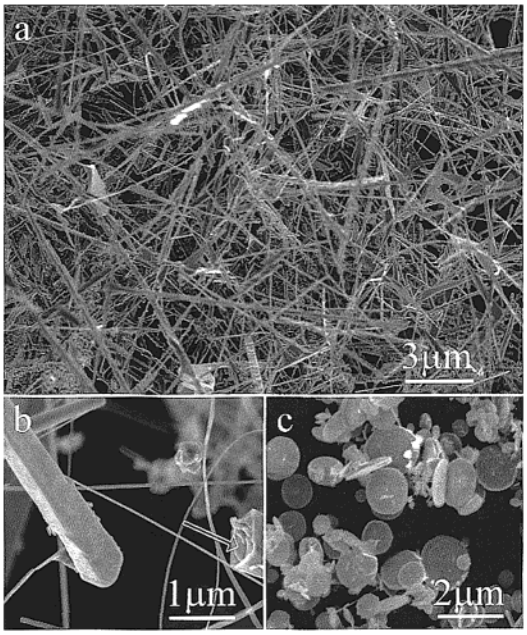

Figure 1. (a) SEM image showing the morphology of the as-synthesized products for the Sn/SnO system (deposited on inner wall of the concentric alumina tube). (b) Enlarged SEM image of a local area for image (a). The sample was made using a layered Sn foil/SnO mixture. The synthesis was conducted at a furnace temperature at the central region of 1125 °C and a chamber pressure of 400 Torr at a flow rate of 100 sccm. The sample was collected from the walls of the concentric tube. (c) SEM image showing disklike products formed on a cold plate central to the upstream region of the flow system. See text for discussion.

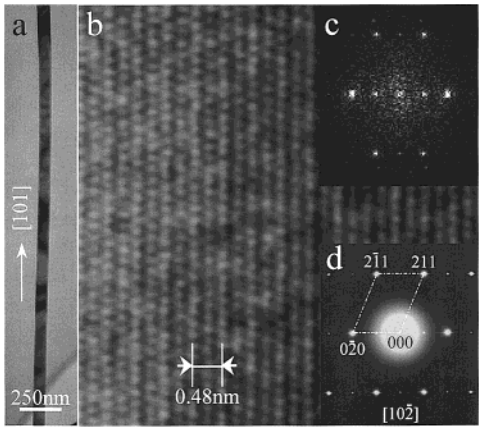

Figure 2. (a) Low magnification TEM image of a rutile structured SnO_2 nanowire. (b) High-resolution TEM image of the nanowire. (c) Corresponding FFT of the image, and (d) SAD pattern from the nanowire. See text for discussion.

characterize the sample collected at considerably lower temperatures on the cold plate. The typical diameter of these disks is 1−2 μm with a thickness of several tens of nanometers. Some tiny nanodisks are also identified. The chemical composition of these disks, however, corresponds to SnO and not SnO_2. In the present paper, we will focus on the study of the wire-like nanostructures produced as the as-synthesized products of primarily the Sn/SnO synthesis.

3.2 Tetragonal (Rutile) Structured SnO_2 Nanowires. All of the wire-like products including those several tens of nanometers in diameter (Figure 2(a)) are found to be straight. We have investigated the crystallography of these SnO_2 nanowires using select area electron diffraction (SAD) (Figure 2(d)) and HRTEM imaging (Figure 2(b)) combined with a fast Fourier

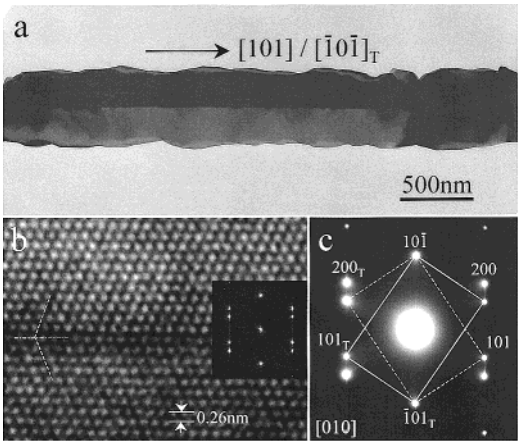

Figure 3. (a) TEM image of an SnO_2 nanowire with twin structure, (b) HRTEM image of the twin, where the inset is the corresponding FFT of the image. (c) Electron diffraction pattern from the nanowire shown in (a). The sample was made by vaporizing an SnO powder sample at a furnace temperature of 1050 °C and a chamber pressure (argon) of 250 Torr. The sample was collected from a cold plate placed in the flow channel.

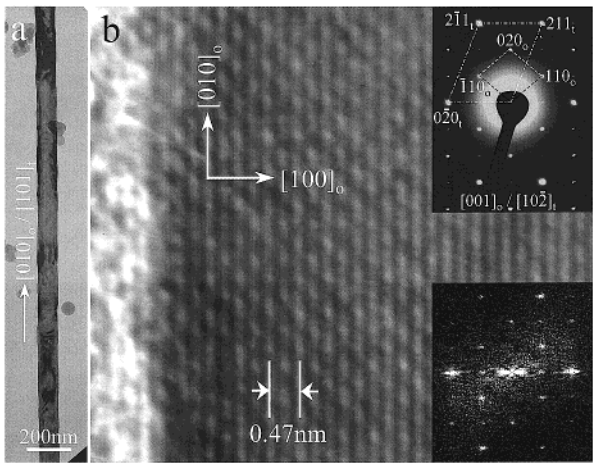

Figure 4. (a) Low magnification TEM image of an individual orthorhombic SnO_2 nanowire, and (b) the corresponding HRTEM image. The inset at the upper right-hand corner is a select area electron diffraction pattern obtained for the nanowire shown in (a) and the inset at the bottom right-hand corner is a FFT of the HRTEM image. The sample was made using a layered Sn foil/SnO reactant mixture. The furnace temperature was 1050 °C and the chamber pressure 200 Torr. The sample was collected from the cold plate after being deposited at 25 °C.

transform (FFT) analysis technique (Figure 2(c)). The results indicate that the SnO_2 nanowires have a normal rutile crystal structure ($a = 0.470$ nm, and $c = 3.188$ nm).[17] This crystallographic configuration of the SnO_2 nanowires is similar to that of the previously observed SnO_2 nanobelts.[3,4] The SnO_2 nanowires can also display a rectangular cross section enclosed by $\pm(010)$ and $\pm(10\bar{1})$ facet planes, and a thickness-to-width aspect ratio ranging from 1:2 to 1:5, which is smaller than that for the SnO_2 nanobelts (1:5−1:10).[3,4] The growth direction of these SnO_2 nanowires is parallel to the [101] crystal direction.

As we find that the diameter of the nanowires varies from wire to wire over a broad range, we observe that structural defects are introduced especially in the nanowires of large diameter. Figure 3(a) depicts the TEM image of an SnO_2 nanowire with a single twin structure. The corresponding SAD pattern is shown in Figure 3(c). Here, the "twin" reflections are indexed with a subscript "T" and the remaining matrix reflection indices are marked without subscript. The zone axis of the diffraction pattern is [010] for the rutile structured SnO_2. The twinning plane is determined to be $(10\bar{1})$ and the twinning direction is [101], parallel to the growth direction of the SnO_2 nanowire. The twin also can be regarded as being formed by one part of the crystal (twin) rotated 180° along the normal direction of the $(10\bar{1})$ crystal plane while the remaining sections of the crystal (matrix) maintain the original orientation. Shown in Figure 3(b) is a HRTEM image around the twin boundary that is completely coherent, with no relative displacement. The inset corresponds to the FFT of the HRTEM image, which is consistent with the experimental electron diffraction pattern given in Figure 3(c).

3.3 Orthorhombic Structured SnO_2 Nanowires. In complement to the normal rutile structured SnO_2 nanowires, we have found that some of the additional SnO_2 nanowires display a crystal structure different from rutile SnO_2. Depicted in Figure 4(a) is a low magnification TEM image of one of these SnO_2 nanowires. Figure 4(b) is the corresponding HRTEM image. The inset at the upper right-hand corner of Figure 4(b) is an experimental SAD pattern. A matched pattern is reproduced by the FFT of the HRTEM image, as inserted at the bottom right-hand corner of Figure 4(b). The configuration of the reflections with strong intensities in the SAD pattern (inset) is the same as that for the $[10\bar{2}]$ crystal zone of rutile structured SnO_2 (Figure 2(d)). Some extra weak reflections, however, are clearly seen in the SAD pattern inserted in Figure 4(b). Their geometrical configuration is commensurate to that of the strong reflections, indicating the formation of a superlattice structure (or superstructure) associated with the normal rutile SnO_2. The superstructure is determined to match that of orthorhombic structured SnO_2 having the lattice parameters: $a = 0.4714$ nm, $b = 0.5727$ nm, and $c = 0.5214$ nm. This observation is somewhat surprising as previous bulk phase studies suggest that the orthorhombic structure is formed only under high-pressure conditions.[18] The SAD pattern corresponds to the $[001]_o$ crystal zone of the orthorhombic SnO_2 superstructure. The indexes with a subscript "o" correspond to the ortho-rhombic SnO_2 superstructure, whereas the basic reflections indexed on the basis of the normal rutile structured SnO_2 are denoted with a subscript "t". The determined orientation relationship between the orthorhombic SnO_2 and the tetragonal (rutile) SnO_2 corresponds to $[001]_o \,||\, [10\bar{2}]_t$ and $(100)_o \,||\, (010)_t$. Assuming the cross-sectional shape of the nanowire is rectangular, the orthorhombic SnO_2 nanowire is enclosed by $\pm(100)_o/\pm(010)_t$ and $\pm(001)_o/\pm(10\bar{1})_t$, its growth direction being along the $[010]_o$ crystal direction that is parallel to $[101]_t$ of the rutile structured SnO_2.

3.4 Sandwiched SnO_2 Nanoribbons. Another typical morphology observed for the wire-like nanostructures is shown in Figure 5(a). Here, the nanostructure consists of two side layers whose thickness is about 20 nm and a core layer with a width ~120 nm. Considering the contrast over the length of the nanostructure and the results of chemical imaging, the wire-like nanostructure is found to have a rectangular cross section with a smaller aspect ratio than that observed previously for the nanobelts.[3] It is, therefore referred to as a sandwiched nanoribbon to distinguish it from the nanobelts.[3] Although small parts of the side layers are missing, the nanoribbon appears to have a generally uniform width over its entire length. The composition of the sandwiched nanoribbon also approaches that of SnO_2 as determined by EDS. The SAD pattern (Figure 5(b)) indicates that the nanoribbon is not a purely rutile structured SnO_2 but likely has significant orthorhombic structure (SnO_2) because the super-reflections corresponding to orthorhombic SnO_2 are observed. To further understand the crystal structure

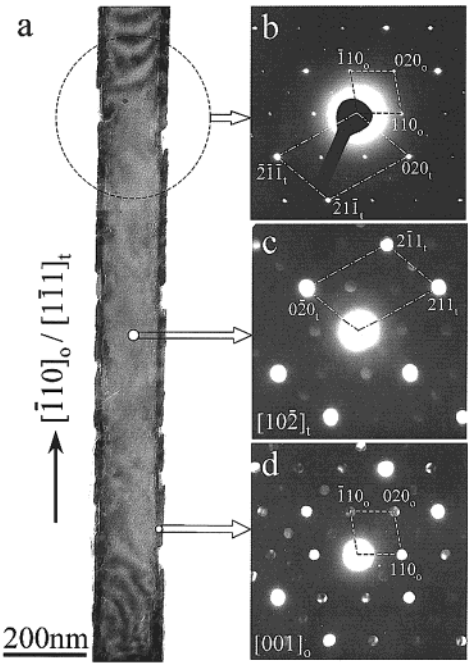

Figure 5. (a) TEM image of an individual sandwiched nanoribbon. (b) Select area electron diffraction pattern from the ribbon, (c,d) Micro-diffraction patterns taken from the center and edge of the nanoribbon, respectively. The sample was made using a layered Sn foil/SnO reactant mixture. The furnace temperature was 1050 °C as the chamber ranged from 250 to 700 Torr over the course of the run. The sample was collected from the cold plate. See text for discussion.

of the nanoribbon, electron micro-diffraction patterns have been recorded for the core layer (Figure 5(c)) and side layer (Figure 5(d)), respectively. Evidently, the reflections corresponding to the rutile structured SnO_2 are very strong in the micro-diffraction pattern taken of the center of the core layer (Figure 5(c)) although weak reflections corresponding to orthorhombic SnO_2 can be identified. The micro-diffraction pattern from the side layer (Figure 5(d)), however, displays a notably stronger diffraction feature for orthorhombic SnO_2.

The results imply that the nanoribbon core layer is likely to adopt the rutile structure, whereas the side layers adopt predominantly the orthorhombic structure. The superlattice reflection observed in the pattern recorded from the center of the nanoribbon may come from the top and bottom surface layers that are dominated by the orthorhombic structure. The HRTEM image recorded near the edge layer displayed in Figure 6, and the corresponding FFT given in the inset verifies that orthorhombic structured SnO_2 is formed in the edge layer. The surface of the SnO_2 nanoribbon edge is not flat at the atomic level, as indicated by its HRTEM image (Figure 6). The orthorhombic SnO_2 and the normal rutile SnO_2 are coherent with orientation relationships: $[001]_o \parallel [10\bar{2}]_t$ and $(100)_o \parallel (010)_t$. This is virtually the same relationship as that deduced for the corresponding orthorhombic SnO_2 nanowires considered in Section 3.3. The sandwiched SnO_2 nanoribbons, however, are enclosed by $\pm(110)_o/\pm(231)_t$ and $\pm(001)_o/\pm(10\bar{1})_t$, and their growth directions are parallel to $[\bar{1}10]_o/[1\bar{1}1]_t$.

The contrast over sandwiched SnO_2 nanoribbons with smaller widths, similar to that shown in Figure 6(a), is, in general, uniform. With an increase in width, however, the contrast over the nanoribbons becomes complex, as indicated in Figure 7, parts a and b, where two sandwiched nanobands with width of order 500 nm are displayed. One of the nanobands (Figure 7(b)) has only one side layer. The thickness of the surface layers does not significantly increase as the width of the nanoribbon

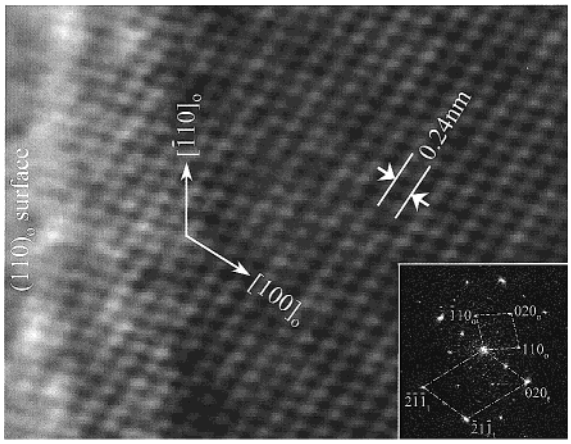

Figure 6. (a) HRTEM image of the edge area of the sandwiched nanoribbon shown in Figure 5(a). Inset is the FFT of the corresponding image.

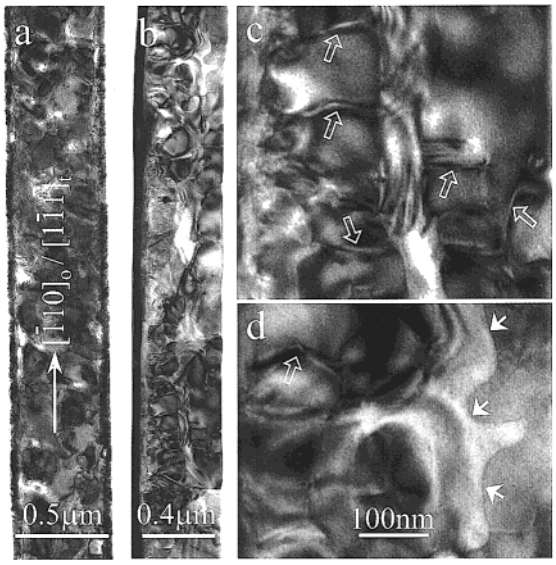

Figure 7. (a) and (b), correspond to TEM images of two wide nanoribbons, and (c) and (d) are enlarged images showing the detailed microstructures of the nanoribbons. The sample was made using SnO powder at a furnace temperature of 1050 °C, a chamber pressure of 250 Torr, and the sample was collected from a coldfinger placed in the channel.

increases. Although the contrast displayed is complicated, the entire nanoribbon is single crystalline and the SAD pattern is identical to that given in Figure 5(b). Shown in Figure 7(c)−(d) are two enlarged images of local areas in the nanoribbon (Figure 7(b)). Here, dislocations can be identified, as indicated by the open arrowheads.

In addition, a domain-like boundary can also be identified in the nanoribbon, as marked by solid arrowheads in Figure 7(d). Figure 8 corresponds to an HRTEM image associated with the boundary region. This indicates that a domain boundary is formed by the rutile structured SnO_2 (t-SnO_2) and the orthorhombic structured SnO_2 (o-SnO_2). The boundary is semi-coherent and not abrupt on the atomic scale. The dash line marked in Figure 8 represents this boundary schematically. These observations thus suggest that the large width nanoribbons correspond to a mixed phase SnO_2, where dislocations and domain boundaries coexist.

Bulk orthorhombic SnO_2 has been synthesized at a high pressure of 158 kbar.[18] Although its lattice parameters have been determined, the atomic positions in the crystal have not been

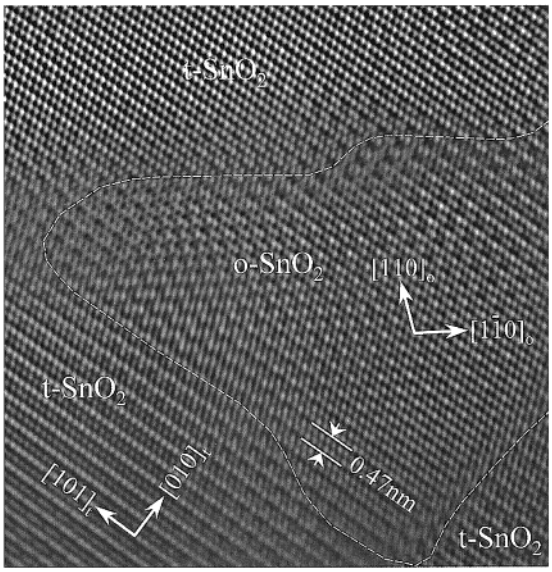

Figure 8. HRTEM image showing the domains formed by rutile-SnO_2 and orthorhombic-SnO_2 in the nanoribbons displayed in Figure 7.

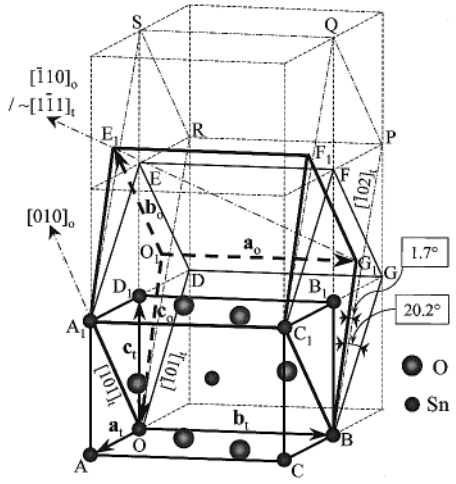

Figure 9. Schematic diagram of the crystal structures of rutile SnO_2 and orthorhombic SnO_2, where the a_t, b_t, and c_t represent the base vectors of the rutile structured SnO_2, and the a_o, b_o, and c_o denote the base vectors for the orthorhombic SnO_2.

reported. To understand the structural relationship between the orthorhombic and normal rutile SnO_2, a schematic diagram of the crystal structures is presented in Figure 9. This figure is constructed on the basis of the orientation relationships between the two structures that we have determined in the present study. The rectangular parallelepiped $BOAC-B_1D_1A_1C_1$ represents a unit cell for the rutile structured SnO_2 crystal. Here, the large spheres denote oxygen atoms and small spheres tin atoms. Six unit cells of rutile SnO_2 are drawn in the diagram, as indicated by the dotted lines. The rectangular parallelepiped A_1OBC_1-$E_1O_1G_1F_1$ is a unit cell for the orthorhombic SnO_2. This unit cell of the orthorhombic SnO_2 can be regarded as forming from the parallel-piped A_1OBC_1-EDGF in the rutile structured SnO_2 by shearing along the $[101]_t$ crystal direction, followed by a slight compression along the *c*-axis of orthorhombic SnO_2. The shearing angle is 20.2°, and the compression in length is 1.6%. The dimensions of the *a*-axis and *b*-axis of the orthorhombic SnO_2 are also adjusted very slightly (0.5% compression in the *a*-axis and 0.3% expansion in the *b*-axis) relative to the corresponding spacing distances in the rutile SnO_2 structure.

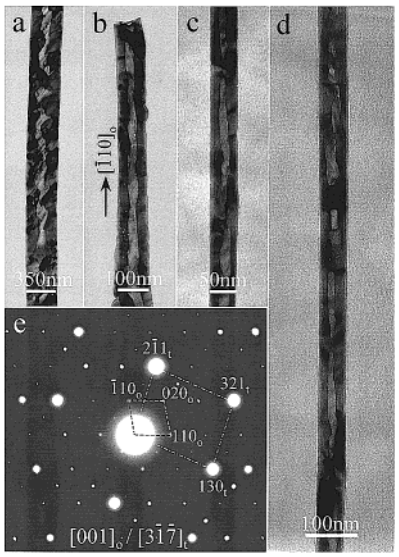

Figure 10. (a), (b), and (c) are TEM images of SnO_2 nanotubes, and (d) a select area electron diffraction pattern taken for the SnO_2 nanotube shown in (b). The sample was made using SnO powder at a furnace temperature of 1100 °C, a chamber pressure of 250 Torr, and the sample was collected from the walls of the tube furnace.

The volume decrease is 1.8%. The volume change results in the semi-coherent boundary between the orthorhombic and rutile structured SnO_2 (Figure 8) and might be responsible for the missing parts of the side layers in the sandwiched SnO_2 nanoribbon shown in Figure 5. The $[001]_o$ (*c*-axis) crystal direction is not exactly parallel to $[10\bar{2}]_t$. Instead, there is an included angle of 1.7° between $[001]_o$ and $[10\bar{2}]_t$, which can be barely detected from the select area electron diffraction patterns shown in Figures 4 and 5(b). The growth directions of the wire-like nanostructures are also indicated as $[010]_o/[101]_t$ and $[\bar{1}10]_o/[1\bar{1}1]_t$.

3.5 SnO_2 Nanotubes. Figure 10(a)−(c) corresponds to TEM images showing yet another characteristic of the wire-like nanostructures observed in the present as-synthesized samples. The chemical composition of these wire-like nanostructures also corresponds to SnO_2. The bright contrast for the center part of the wire-like nanostructures is always accompanied by the dark sides even with tilting of the sample under TEM observation. This indicates that the wire-like nanostructures have hollow cores, i.e., they correspond to SnO_2 nanotubes. The diameter size of the SnO_2 nanotubes varies from 50 nm (Figure 10(c)−(d)) to 350 nm (Figure 10(a)) and their typical length is several micrometers. The hollow core is not always continuous through the entire length of the sample, especially for those nanotubes of smaller (diameter) size (Figure 10(c)−(d)). For the SnO_2 nanotubes with large diameters, the hollow core displays a zigzag shape (Figure 10(a)).

Electron diffraction analyses indicate that the SnO_2 nanotubes correspond to a single crystal. Shown in Figure 10(e) is an SAD pattern taken for the SnO_2 nanotube depicted in Figure 10(b). Here, the reflections with strong intensities are indexed to belong to the$[31\bar{7}]_t$ zone axis of the rutile structured SnO_2, and the weak reflections correspond to an orthorhombic SnO_2 superstructure along the $[001]_o$ zone axis. The orientation relationship between the orthorhombic SnO_2 and the rutile SnO_2 structures is determined to be $[001]_o \,||\, [3\bar{1}\bar{7}]_t$ and $\pm(110)_o \,||\, (451)_t$. If we consider only the orthorhombic SnO_2, the growth direction of the SnO_2 nanotubes is parallel to $[\bar{1}10]_o$, identical to that of the SnO_2 sandwiched nanoribbons.

4. Summary

In this study, we have demonstrated the synthesis of both rutile and orthorhombic crystalline tin oxide (SnO_2) nanostructures in the form of nanowires, nanoribbons, and nanotubes we have used two starting products, primarily interlayered Sn foil/SnO mixtures or simply SnO powders. The system used in this study operates from a base pressure of 20 milliTorr as the pressure ranges given in Table 1 correspond primarily to total pressures (Ar, N_2 ...) obtained with 100 sccm entrainment gas flows under adjustable "baffled" forepumping of the system.

There are several important factors which distinguish the present study. First and foremost is our ability to synthesize an orthorhombic ($a = 0.4714$ nm, $b = 0.5727$ nm, $c = 0.5214$ nm) SnO_2 "superlattice" structure at nominal pressures (primarily N_2). If we compare the results that we obtain for the SnO only and interleaved Sn foil/SnO synthesis mixtures, then we find that the latter combination greatly increases our ability to produce SnO_2 nanowires. The data in Figure 4, which displays a strong SAD pattern associated with the rutile SnO_2 structure and weak reflections associated with the orthorhombic "superlattice" structure, in conjunction with our initial synthesis materials suggests the possibility that the weak structure may, in fact, be associated with an oxygen deficiency in the synthesized SnO_2. The orthorhombic and rutile structures of SnO_2 do display very similar unit cell parameters suggesting that the orthorhombic structure might be readily converted.

It is relevant that the "fluffy" gray to gray-black material which we synthesize can be converted through controlled heating at ~1100 °C under a 1% oxygen/UHP Argon flow to a somewhat more dense white SnO_2 powder (the same synthesis product mixture under an Ar (4% H_2) flow is reduced completely to metallic tin). The present results are therefore consistent with the observations made in the SnO-based nanobelt synthesis,[3] where only a rutile SnO_2 crystal structure is observed, if we assume that the present experiments, especially those involving Sn foil/SnO, result in an oxygen deficient product synthesis. We suggest that the ability to produce the orthorhombic superlattice structure, if it results from an oxygen deficient environment, may have important implications for syntheses in similar systems. These will be the subject of future study in our laboratory.

References and Notes

(1) Morales, A. M.; Lieber, C. M. *Science* **1998**, *279*, 208.
(2) Yu, D. P.; Bai, Z. G.; Feng, S. Q.; Lee, C. S.; Bello, I.; Sun, X. S.; Tang, Y. H.; Zhou, G. W.; Zhang, Z. *Solid State Commun.* **1998**, *105*, 403.
(3) Pan, Z. W.; Dai, Z. R.; Wang, Z. L, *Science* **2001**, *291*, 1947.
(4) Dai, Z. R.; Pan, Z. W.; Wang, Z. L. *Solid State Commun.* **2001**, *118*, 351.
(5) Tatsuyama, C.; Ichimura, S. *Jpn. J. Appl. Phys.* **1976**, *15*, 843.
(6) Aoki, A.; Sasakura, H. *Jpn. J. Appl. Phys.* **1970**, *9*, 582.
(7) Watson, J. *Sens. Actuators* **1984**, *5*, 29.
(8) Yamazoe, N. *Sens. Actuators B* **1991**, *5*, 7.
(9) Sberveglieri, G. *Sens. Actuators B* **1992**, *6*, 239.
(10) Dieguez, A.; et al. *Sens. Actuators B* **1996**, *31*, 1.
(11) Ansari, S. G.; et al. *Thin Solid Films* **1997**, *295*, 271.
(12) Nayral, C.; et al. *Appl. Surf. Sci.* **2000**, *164*, 219.
(13) Pan, Z. W.; Dai, Z. R.; Wang, Z. L. *Appl. Phys Lett.* **2000**, submitted.
(14) Lee, S. T.; Wang, N.; Zhang, Y. F.; Tang, Y. H. *MRS Bulletin* **1999**, *24*, 36.
(15) Gole, J. L.; Stout, J. D.; Rauch, W. L.; Wang, Z. L. *Appl. Phys. Lett.* **2000**, *76*, 2346.
(16) Wang, Z. L.; Gao, R. P.; Gole, J. L.; Stout, J. D. *Adv. Mater.* **2000**, *12*, 1938.
(17) Baou, W. H. *Acta Crystallogr.* **1956**, *9*, 515.
(18) Suito, K.; Kawai, N.; Masuda, Y. *Mater. Res. Bull.* **1975**, *10*, 677.